Available online at www.sciencedirect.com

SciVerse ScienceDirect

Ceramics International 38 (2012) 5305–5310

CERAMICS INTERNATIONAL

www.elsevier.com/locate/ceramint

Short communication

Controlled synthesis of Eu^{2+}-doped barium silicate nanostructures and their optical properties

Zhengwu Lu [a,*], Luqian Weng [a], Shenhua Song [a], Peixin Zhang [b,**], Xiongbiao Luo [b], Xiangzhong Ren [b]

[a] *Materials Science and Engineering, Shenzhen Graduate School, Harbin Institute of Technology, Xili, Shenzhen 518055, China*
[b] *School of Chemistry and Chemical Engineering, Shenzhen University, Shenzhen 518060, China*

Received 10 February 2012; accepted 29 February 2012
Available online 7 March 2012

Abstract

Several shapes of Eu^{2+}-doped barium silicate nanostructures have been simply obtained by a hydrothermal method. Hedgehog-like, spherical-shaped, porous irregular spherical, hollow worm-like, and cracked worm shell-like structures are synthesized with changing the molar ratios of Ba/Si in solution. The possible formation mechanisms of these barium silicate nanostructures are proposed. Under an excitation wavelength of 360 nm, all the products show broad emission bands from about 400 to 625 nm. The UV region excitation band from 300 to 400 nm confirms the possibility that the nanostructures could be used as phosphors for white LEDs.

Keywords: C. Optical properties; Barium silicate; Hydrothermal; Nanostructures

1. Introduction

Luminescent nanostructured materials have attracted a lot of interest in recent years because of their excellent properties shown in luminescent devices [1], optical amplifiers [2], and as fluorescent labels for biomolecules [3]. Among available luminescent materials, rare-earth-doped inorganic luminescent materials involve a large number of compounds with specific properties. Considerable efforts have been devoted to the morphological control and the understanding of the correlations between the properties of these compounds and their structures and morphologies [4–6].

As host lattices, barium-based silicates (BSOs) have attracted much attention owing to their outstanding thermal and chemical stability and structural diversity. Rare-earth-doped BSOs serve as an important class of phosphors for solid-state light-emitting devices (LEDs), florescent lamps, and plasma display panels (PDPs) [7,8]. From the structural point of view, the BSOs can be considered as $BaO–SiO_2$ systems, in which rare-earth ions with the same valence and a similar radius, such as Eu^{2+} ions, can substitute for Ba^{2+} sites in the lattices and form a stable doped compound. As with the host lattices, activators also play an important role in the performance of luminescent materials. Eu^{2+} ion is a well-known activator in most prominent luminescent materials since the emission of the rare-earth Eu^{2+} ion relies on allowed $5d–4f$ transitions. Moreover, the emission wavelength of Eu^{2+} ranges usually from violet to red due to the $4f^6 5d \rightarrow 4f^7$ transition, coupled to the host crystal field (oxides, nitrides, or sulfides) [9].

Herein, we report a simple hydrothermal approach to the synthesis of several morphologies of the Eu^{2+}-doped barium silicate nanostructures. By controlling the reaction conditions, the products with different shapes can be obtained, such as hedgehog-like particles (S1), spherical-shaped particles (S2), porous irregular spherical particles (S3), hollow worm-like particles (S4), and cracked worm shell-like particles (S5). Finally, intensive bluish-white emissions excited efficiently by UV light were observed from all the products, implying that the Eu^{2+}-doped barium silicate nanostructures may become potential down-conversion phosphors excited by UV-LEDs.

* Corresponding author. Fax: +86 755 26033504.
** Corresponding author.
E-mail addresses: lu.zhengwu@hitsz.edu.cn (Z. Lu), pxzhang96@yahoo.com (P. Zhang).

0272-8842/$36.00
doi:10.1016/j.ceramint.2012.02.095

2. Experimental

Barium nitrate ($Ba(NO_3)_2$, >99%, Kermel Chemical Reagent, Tianjin, China), Tetraethylorthosilicate (TEOS, >99%, Damao Chemical Reagent, Tianjin, China), ethylenediamine (EDA, $H_2NCH_2CH_2NH_2$, >99%, Baishi Chemical Reagent, Tianjin, China), europium nitrate pentahydrate ($Eu(NO_3)_3{\cdot}5H_2O$, >99%, Rare-chem hi-tech, Huizhou, China), and hydrazine hydrate ($N_2H_4{\cdot}H_2O$, >80%, Damao Chemical Reagent, Tianjin, China) with analytical purity were used.

In a typical procedure, 1.96 mmol $Ba(NO_3)_2$ and 0.04 mmol $Eu(NO_3)_3{\cdot}5H_2O$ were dissolved in 20 mL distilled water and the mixture was stirred for 1 h. TEOS (3 mmol) was dissolved in 50 mL ethylenediamine solution (45 mL EDA + 5 mL distilled water) and also stirred for 1 h. Then the TEOS solution was added to the previous solution and stirred again for 2 h. In the obtained solution, 2 mL of 80% $N_2H_4{\cdot}H_2O$ solution was added to offer a reducing atmosphere due to its reducibility. Finally, the above mixture was transferred into a Teflon-lined 100 mL autoclave and maintained for 20 h at 180 °C. This sample was denoted as sample 1 (S1). For synthesizing of S2–S5, the molar ratio of starting materials $Ba(NO_3)_2$ and TEOS was changed regularly. The product was collected by filtration and washed with distilled water and ethanol several times. Then, the samples were obtained after dried at 60 °C for 6 h. A brief summary of the detailed experimental conditions is listed in Table 1.

The morphology and size of the samples were characterized using field emission scanning electron microscopy (FESEM, Hitachi S-4700). Crystal structures of the samples were examined by means of X-ray diffraction (XRD) with a Rigaku D/max 2500 diffractometer (Cu K_α radiation, $\lambda = 0.15405$ nm). The data were collected over a 2 theta range from 10° to 60° at a scanning speed of 0.05° s^{-1}. Energy dispersive X-ray (EDX) spectrometry equipped in the FESEM was used to determine the sample compositions. The photoluminescence (PL) emission and excitation spectra were carried out with a Shimadzu (RF-5301PC) fluorescent spectrometer via a xenon lamp at room temperature.

3. Results and discussion

3.1. Morphological, structural and compositional analyses

The FESEM images of the obtained products are shown in Fig. 1. By adjusting the molar ratio of the starting materials Ba and Si, five kinds of morphologies are obtained. In the beginning, the Si content was kept constant, and the Ba content was increased. At Ba:Si ≈ 2:3, a kind of hedgehog-like particles (S1) with a high yield could be obtained (Fig. 1a). The particle is composed of nanoplates with a size of about 50–100 nm (Fig. 1b). When the molar ratio of Ba:Si is about 3:3, solid spherical-shaped particles (S2) were synthesized. From Fig. 1c, it is seen that two or three of these spherical particles closely contact with each other. The high-magnification FESEM in Fig. 1d reveals that the sample is composed of nanorods with a diameter of about 100 nm, and a small number of nanorods with different lengths are also observed on the surface of the sample. When the Ba:Si ratio is increased to about 6:3, irregular spherical particles with small holes (S3) were obtained (Fig. 1e). The sample is also composed of numerous nanorods with larger sizes (Fig. 1f). Fig. 1g and h shows the FESEM images of the products (S4) obtained by increasing the Si content, while maintaining the Ba content (Ba:Si ≈ 6:6). The low-magnification FESEM image in Fig. 1g reveals that the obtained product is high-yield worm-like structures. The corresponding high-magnification FESEM (Fig. 1h) indicates that the product is composed of nanoparticles with an average size of about 200 nm and its one end is hollow. With further increasing Si content (Ba:Si ≈ 6:10), cracked worm shell-like particles (S5) were obtained (Fig. 1i). The typical high-magnification FESEM image (Fig. 1j) shows that the cracked worm shell-like particles contain some solid irregular particles inside.

Organic additives with functional groups, e.g., amino groups, are thought to regulate crystal nucleation and growth, modulate crystal shape and size, and control the organization of nanoscale building blocks into complex structures [10–12]. Ethylenediamine (EDA) is a bidentate ligand consisting of amino groups. The polarity and ligand of EDA can successfully control the growth of the crystals [13]. In our work, EDA could be coupled with barium ions in the form of complex ions dispersed in solution [14]. It was also used as the source of hydroxide ions based on ionization, while the source of silicate ions was provided by using TEOS, which could be dissolved in an alkaline condition. According to the FESEM images (Fig. 1), it can be presumed that the formation procedure is an EDA-assisted self-organization process. Although the exact roles of EDA in the morphological control are still not completely understood, the EDA might play a role as follows. Firstly, barium ions and silicate ions were protected by the EDA via hydrogen bonding between ions and EDA amino groups. As the reaction proceeded, they might attack each other and form initial barium silicate nanocrystals. These freshly formed

Table 1
Experimental condition for the preparation of the samples.

Samples	Solvent	$Ba(NO_3)_2$	TEOS	$Eu(NO_3)_3{\cdot}5H_2O$	EDA	*T*/°C	Morphology
S1	H_2O	1.96 mmol	0.62 g (3 mmol)	0.04 mmol (2 mol%)	45 mL	180	Hedgehog-like particles
S2	H_2O	2.94 mmol	0.62 g (3 mmol)	0.06 mmol (2 mol%)	45 mL	180	Spherical-shaped particles
S3	H_2O	5.88 mmol	0.62 g (3 mmol)	0.12 mmol (2 mol%)	45 mL	180	Porous irregular spheres
S4	H_2O	5.88 mmol	1.24 g (6 mmol)	0.12 mmol (2 mol%)	45 mL	180	Hollow worm-like particles
S5	H_2O	5.88 mmol	2.08 g (10 mmol)	0.12 mmol (2 mol%)	45 mL	180	Worm shell-like particles

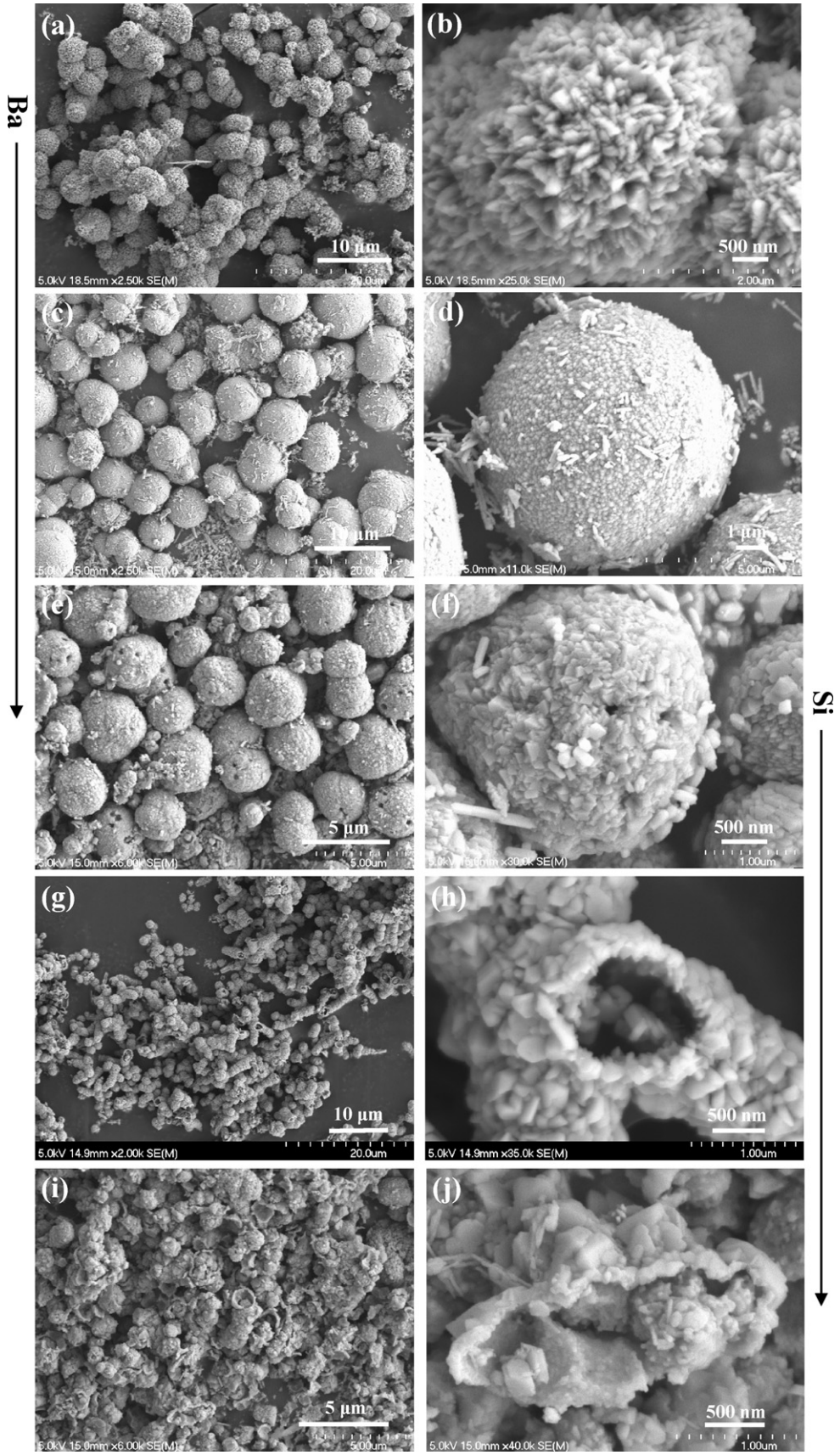

Fig. 1. FESEM images of S1 (a and b), S2 (c and d), S3 (e and f), S4 (g and h), and S5 (i and j).

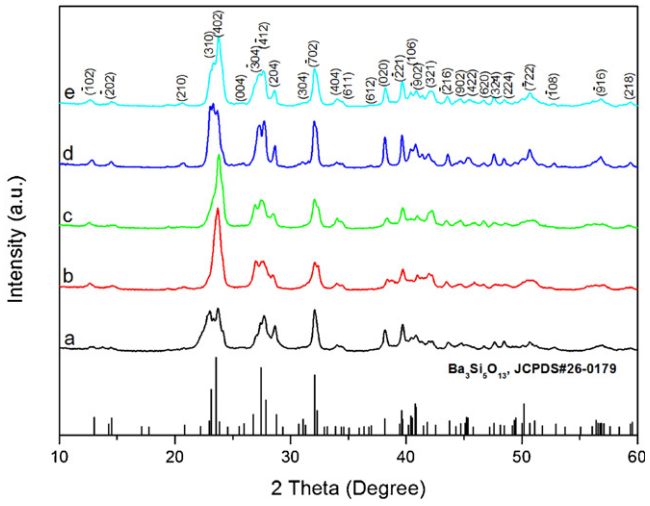

Fig. 2. XRD patterns of the as-prepared products: a (S1), b (S2), c (S3), d (S4), and e (S5).

nanocrystals were unstable and could selectively adsorb EDA due to the high surface activity. The adsorption of EDA on the specific surfaces of barium silicate nanocrystals favors the aggregation of the nanocrystals. The aggregation process is induced by the coalescence process [15,16]. Then the nanocrystals cooperatively assembled and finally agglomerated into different multidimensional microscopic structures.

There were some slight differences among the different products (S1–S5): the sizes of the nanocrystals and the pores were different. In the S1–S3 (Fig. 1a–f), the nanocrystals were primarily 100 nm in diameter, and then became 200 nm in the S4 (Fig. 1g and h). In the S5 (Fig. 1i and j), the diameter of the nanocrystals changed to >200 nm. On the basis of experimental conditions, such a difference should result from changing of the molar ratio of Ba:Si. The growth rate of the nanocrystals was under the control of the concentrations of both barium ions and silicate ions. When their concentrations were low, the growth rate of the nanocrystals was slow and the size was small. The smaller the nanocrystal size, the more compactly they stacked. As the concentrations became high, the nanocrystals grew quickly. Therefore, the nanocrystals were larger at a faster growth rate. However, the larger the nanocrystal size, the harder they stacked compactly. Thus, the diameter of the pore among the nanocrystals became larger from the S3 to S4 until the pore ruptured in the S5.

Fig. 2 shows the XRD patterns of the products prepared by controlling the molar ratio of cations Ba:Si. All of diffraction peaks can be assigned to $Ba_3Si_5O_{13}$ (JCPDS no. 26-0179), with a monoclinic unit cell and $p2_1/c$ space group. The diffraction peaks become stronger and sharper from Fig. 2a–c, which demonstrates a good crystallinity in the as-synthesized products. From Fig. 2c–e, the crystallinity change is not notable. These XRD results reveal that the $Ba_3Si_5O_{13}$ with a high phase purity and good crystallinity can be obtained over a wide range of Ba:Si ratios.

Further evidence was obtained by the energy dispersive X-ray (EDX) spectrometry. A typical EDX spectrum of as-synthesized nanostructures (sample 1) is shown in Fig. 3. As

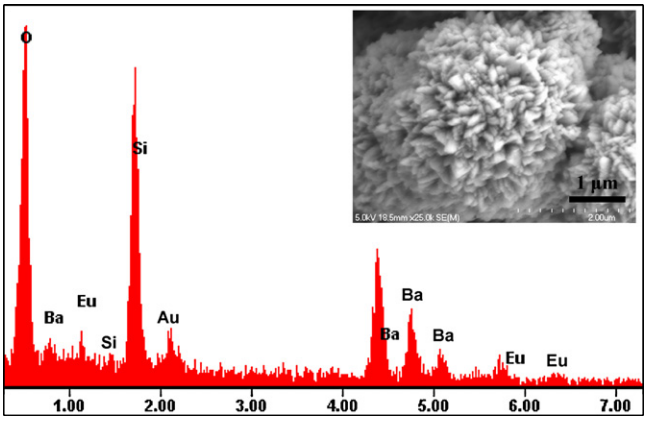

Fig. 3. A typical EDX spectrum of as-synthesized nanostructures (S1).

seen, the spectrum shows visible signals of europium besides barium, silicon and oxygen, suggesting that europium cations had been incorporated into the nanostructures. According to these observations, we believe that europium cations also entered other nanostructures.

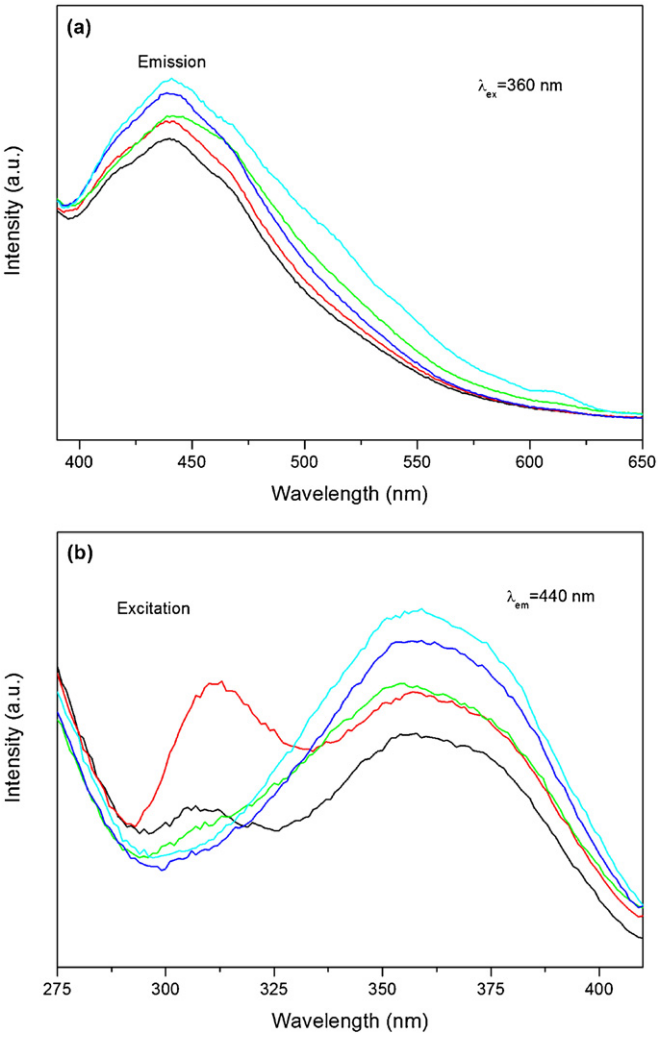

Fig. 4. Room-temperature emission (a) and excitation (b) spectra of S1 (black), S2 (red), S3 (green), S4 (blue), and S5 (cyan). (For interpretation of the references to color in this figure legend, the reader is referred to the web version of this article.)

3.2. Optical analysis

The room-temperature emission and excitation spectra of the doped barium silicate products are depicted in Fig. 4. The emission spectra (Fig. 4a) show broad emission bands from about 400 to 625 nm, covering the blue to orange region, with the maxima at around 440 nm, appearing as a bluish-white color. These broad emission bands should be attributed to the allowed $4f^6 5d \rightarrow 4f^7$ transition of Eu^{2+}. The characteristic luminescence of Eu^{3+} is not observed, which exhibits sharp lines between 580 and 650 nm [17,18]. This suggests that Eu^{3+} was reduced to Eu^{2+} in a reducing atmosphere by using hydrazine hydrate solution. The broad emission appears to be asymmetric, indicating that there are possibly two or more emission peaks. These characteristic features could be ascribed to $Ba_3Si_5O_{13}$ crystal structure as shown in Fig. 5, in which the Ba atoms occupy three kinds of sites (Ba(1), Ba(2), and Ba(3)) [19]. It can be presumed that Eu^{2+} ions occupy different types of sites in the barium silicate host lattice, forming corresponding emission centers. Another possible reason for broad band can be explained by the crystal field splitting effect. The 5*d* levels of Eu^{2+} ions that are not shielded completely by the outer environment split under various ligand field strengths, and the number of split levels is determined by the local symmetry around the Eu^{2+} ions. In the $Ba_3Si_5O_{13}$ compounds, each Ba^{2+} is coordinated by eight oxygen atoms [19], considered as [BaO_8] clusters (Fig. 5), forming a snub disphenoid-type polyhedron with scalenohedral configuration [20]. According to the reported Ba–O interatomic distances (2.75, 2.75, 2.82, 2.85, 2.93, 2.93, 2.97, and 3.02 Å) [19], the barium atoms are not located exactly in the center of the [BaO_8] clusters, and hence a slightly distorted symmetry is preferred. For the substitution of Ba^{2+} ions, Eu^{2+} ions would also form an [EuO_8] distorted geometry. The 5*d* orbits of Eu^{2+} in such an environment could be split into a multilevel. In the emission process, different energy releases would cause peak-overlapping, forming a broad peak.

The peak wavelength of the phosphorescence does not vary with the morphology of the samples. This implies that the

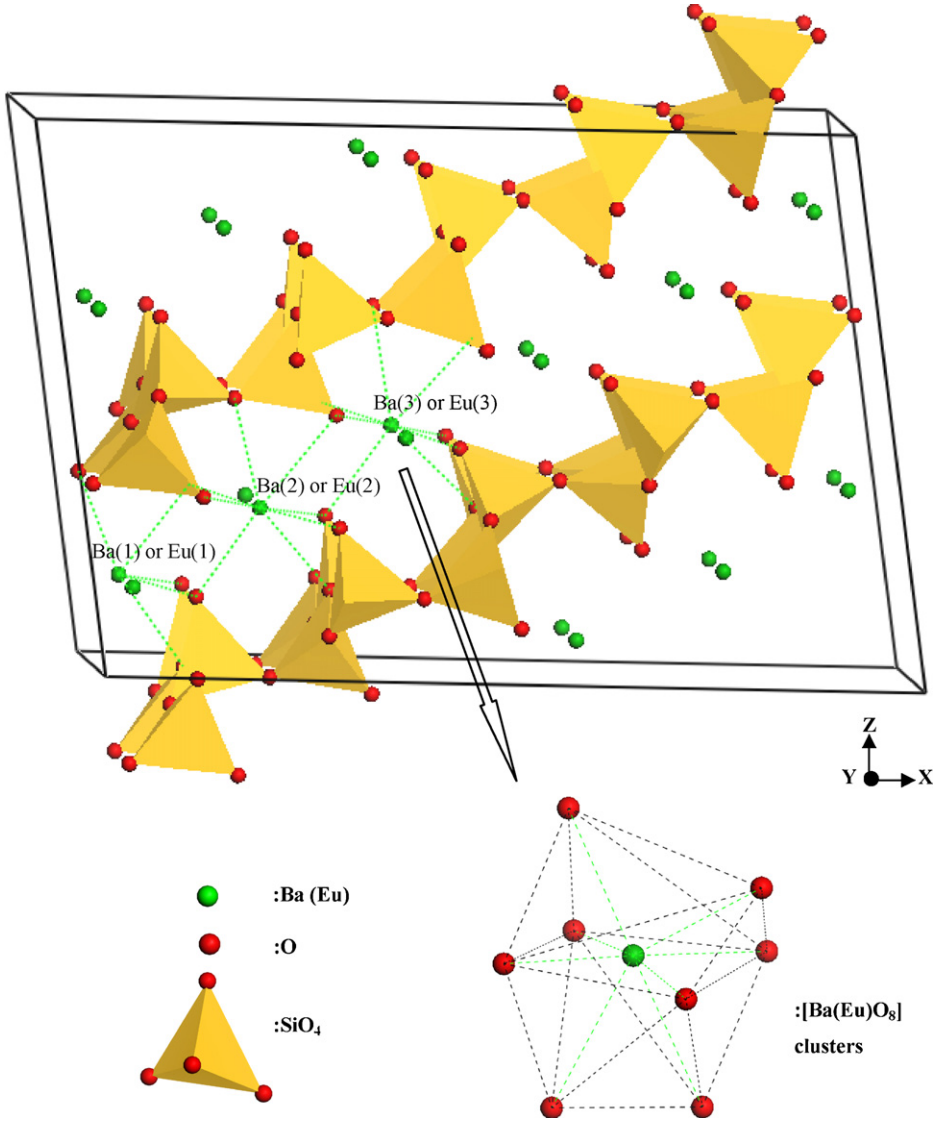

Fig. 5. Crystal structure of monoclinic $Ba_3Si_5O_{13}$ (green spheres, Ba (Eu); red spheres, O; yellow tetrahedron, SiO_4). (For interpretation of the references to color in this figure legend, the reader is referred to the web version of this article.)

crystal field which affects the 5*d* states of Eu^{2+} is not changed by the morphology of the samples, but the intensity of the photoluminescence varies with the morphology. The intensity of the PL should be related to crystallinity and size of the products. Among the five samples, S1 possesses the worst crystallinity and the smallest size, resulting in the lowest emission intensity. Comparatively, the PL intensities of S2–S5 are higher than that of S1; S5 has the highest emission intensity due to its largest size and moderate crystallinity. Fig. 4b shows the excitation spectra of the doped barium silicate products under an emission wavelength of 440 nm. The spectra present broad excitation bands from 300 to 400 nm, which could be corresponding to $4f^7 \rightarrow 4f^6 5d$ adsorption of Eu^{2+}. Two excited levels may possibly exist, since two shoulders are observed at 310 nm and 360 nm on the excitation spectra of S1 and S2. It is noticeable that the excitation band centered at ~310 nm began to weaken, while the band centered at ~360 nm increased gradually from S3 to S5, which provides a promising applicability to the wavelength-conversion phosphors combined with UV-LEDs.

4. Conclusions

Several shapes of Eu^{2+}-doped barium silicate nanostructures are simply prepared through a hydrothermal method. The molar ratio of cations Ba:Si plays a key role in the morphology, crystallinity, and composition of the products. The formation procedure of these barium silicate nanostructures is an EDA-assisted self-organization process. To explain the PL spectra, a model based on the multi-center emissions and the distortion of $[Ba(Eu)O_8]$ clusters is introduced. All the products show a broad emission band from 400 to 625 nm under 360 nm excitation. The excitation band of the phosphors is from about 300 to 400 nm, showing that the as-prepared nanostructures are promising candidates for applications in the white LEDs.

Acknowledgments

This work was financially supported by the National Natural Science Foundation of China (grant nos. 50674068 and 50974090), the Shenzhen Government's Plan of Science and Technology (grant no. JC200903120029A), and the Science and Technology Planning Project of Shenzhen Nanshan District (grant no. 2009037).

References

[1] Z.F. Wang, Y.H. Wang, Y.Z. Li, B.T. Liu, Low dimensional effects on luminescent properties of $CaWO_4$:Tb nanophosphor, J. Electrochem. Soc. 157 (2010) J125–J129.

[2] G.A. Kumar, C.W. Chen, J. Ballato, R.E. Riman, Optical characterization of infrared emitting rare-earth-doped fluoride nanocrystals and their transparent nanocomposites, Chem. Mater. 19 (2007) 1523–1528.

[3] P.R. Diamente, R.D. Burke, F.C.J.M. van Veggel, Bioconjugation of Ln^{3+}-doped LaF_3 nanoparticles to avidin, Langmuir 22 (2006) 1782–1788.

[4] J. Yang, Z.W. Quan, D.Y. Kong, X.M. Liu, J. Lin, Y_2O_3:Eu^{3+} microspheres: solvothermal synthesis and luminescence properties, Cryst. Growth Des. 7 (2007) 730–735.

[5] Z.L. Fu, W.H. Li, S. Du, H.K. Yang, J.H. Jeong, Hydrothermal synthesis and luminescent properties of uniform $CaSnO_3$:Eu^{3+} microcrystals with controlled morphology, J. Electrochem. Soc. 156 (2009) J308–J311.

[6] W.D. Gong, Z.L. Fu, S.H. Zhou, S. Du, S.Y. Zhang, Z.W. Dai, W.H. Li, Template-free hydrothermal synthesis and luminescent properties of octahedral $NaGd(MoO_4)_2$:Eu^{3+} microcrystals, J. Electrochem. Soc. 157 (2010) J338–J341.

[7] C. Ronda, Luminescence, From Theory to Applications, Wiley-VCH, Weinheim, 2008.

[8] J.S. Kim, P.E. Jeon, J.C. Choi, H.L. Park, Emission color variation of M_2SiO_4:Eu^{2+} (M = Ba, Sr, Ca) phosphors for light-emitting diode, Solid State Commun. 133 (2005) 187–190.

[9] P. Dorenbos, Energy of the first $4f^7 \rightarrow 4f^6 5d$ transition of Eu^{2+} in inorganic compounds, J. Lumin. 104 (2003) 239–260.

[10] X.H. Liu, J. Zhang, L.W. Wang, T.L. Yang, X.Z. Guo, S.H. Wu, S.R. Wang, 3D hierarchically porous ZnO structures and their functionalization by Au nanoparticles for gas sensors, J. Mater. Chem. 21 (2011) 349–356.

[11] B. Liu, H.C. Zeng, Mesoscale organization of CuO nanoribbons: formation of dandelions, J. Am. Chem. Soc. 126 (2004) 8124–8125.

[12] L.Y. Chen, Z.D. Zhang, Biomolecule-assisted synthesis of $In(OH)_3$ hollow spherical nanostructures constructed with well-aligned nanocubes and their conversion into C-In_2O_3, J. Phys. Chem. C 112 (2008) 18798–18803.

[13] Y.D. Li, H.W. Liao, Y. Ding, Y. Fan, Y. Zhang, Y.T. Qian, Solvothermal elemental direct reaction to CdE (E = S, Se, Te) semiconductor nanorod, Inorg. Chem. 38 (1999) 1382–1387.

[14] C.R. Wang, K.B. Tang, Q. Yang, C.H. An, B. Hai, G.Z. Shen, Y.T. Qian, Blue-light emission of nanocrystalline CaS and SrS synthesized via a solvothermal route, Chem. Phys. Lett. 351 (2002) 385–390.

[15] L.S. Cavalcante, J.C. Sczancoski, R.L. Tranquilin, J.A. Varela, E. Longo, M.O. Orlandi, Growth mechanism of octahedron-like $BaMoO_4$ microcrystals processed in microwave-hydrothermal: experimental observations and computational modeling, Particuology 7 (2009) 353–362.

[16] J.C. Sczancoski, M.D.R. Bomio, L.S. Cavalcante, M.R. Joya, P.S. Pizani, J.A. Varela, E. Longo, M.S. Li, J.A. Andrés, Morphology and blue photoluminescence emission of $PbMoO_4$ processed in conventional hydrothermal, J. Phys. Chem. C 113 (2009) 5812–5822.

[17] Y.Q. Zhou, J. Liu, X.Y. Yang, X.B. Yu, L.T. Wang, Self-assembly and photoluminescence characterization of $CaMoO_4$:Eu^{3+},Na^+ superstructure via a facile surfactant-free hydrothermal method, J. Electrochem. Soc. 158 (2011) K74–K80.

[18] F. Zhang, Y.H. Wang, Photoluminescence properties of La^{3+}, Eu^{3+} co-doped YVO_4 nanocrystalline powders under VUV/UV excitation, J. Electrochem. Soc. 156 (2009) J258–J262.

[19] K.F. Hesse, F. Liebau, Crystal chemistry of silica-rich barium silicates. I. Refinement of the crystal structures of $Ba_4[Si_6O_{16}]$, $Ba_5[Si_8O_{21}]$ and $Ba_6[Si_{10}O_{26}]$, silicates with triple, quadruple and quintuple chains, Zeitschrift für Kristallographie 153 (1980) 3–17.

[20] J.C. Sczancoski, L.S. Cavalcante, N.L. Marana, R.O. da Silva, R.L. Tranquilin, M.R. Joya, P.S. Pizani, J.A. Varela, J.R. Sambrano, M.S. Li, E. Longo, J. Andrés, Electronic structure and optical properties of $BaMoO_4$ powders, Curr. Appl. Phys. 10 (2010) 614–624.